

Supplementary Information

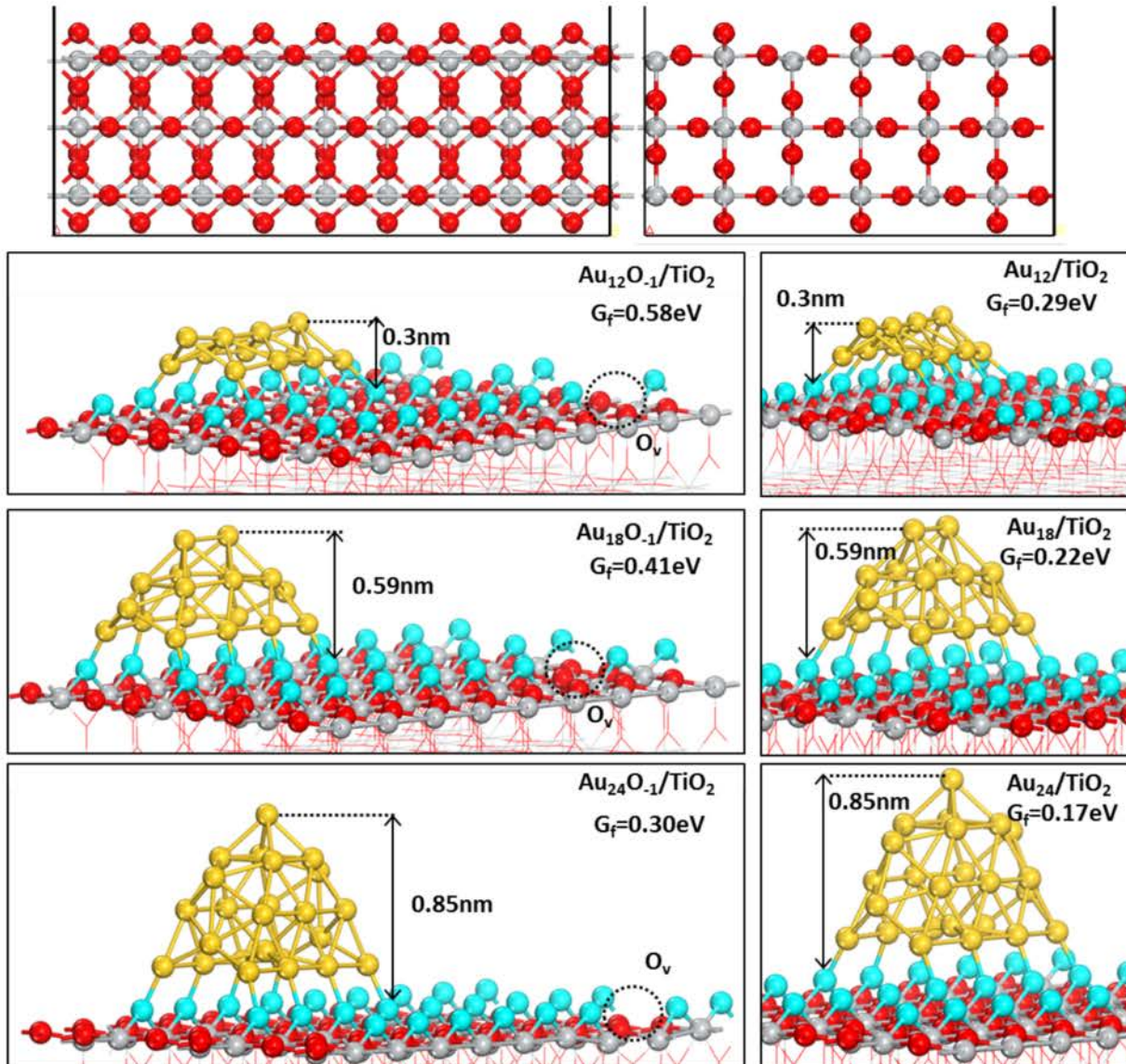
The Dome of Gold Nanolized for Catalysis

Yao Peng,^a Cheng Shang^{a,*} and Zhi-Pan Liu^{a,*}

^a Collaborative Innovation Center of Chemistry for Energy Material, Shanghai Key Laboratory of Molecular Catalysis and Innovative Materials, Key Laboratory of Computational Physical Science, Department of Chemistry, Fudan University, Shanghai 200433, China

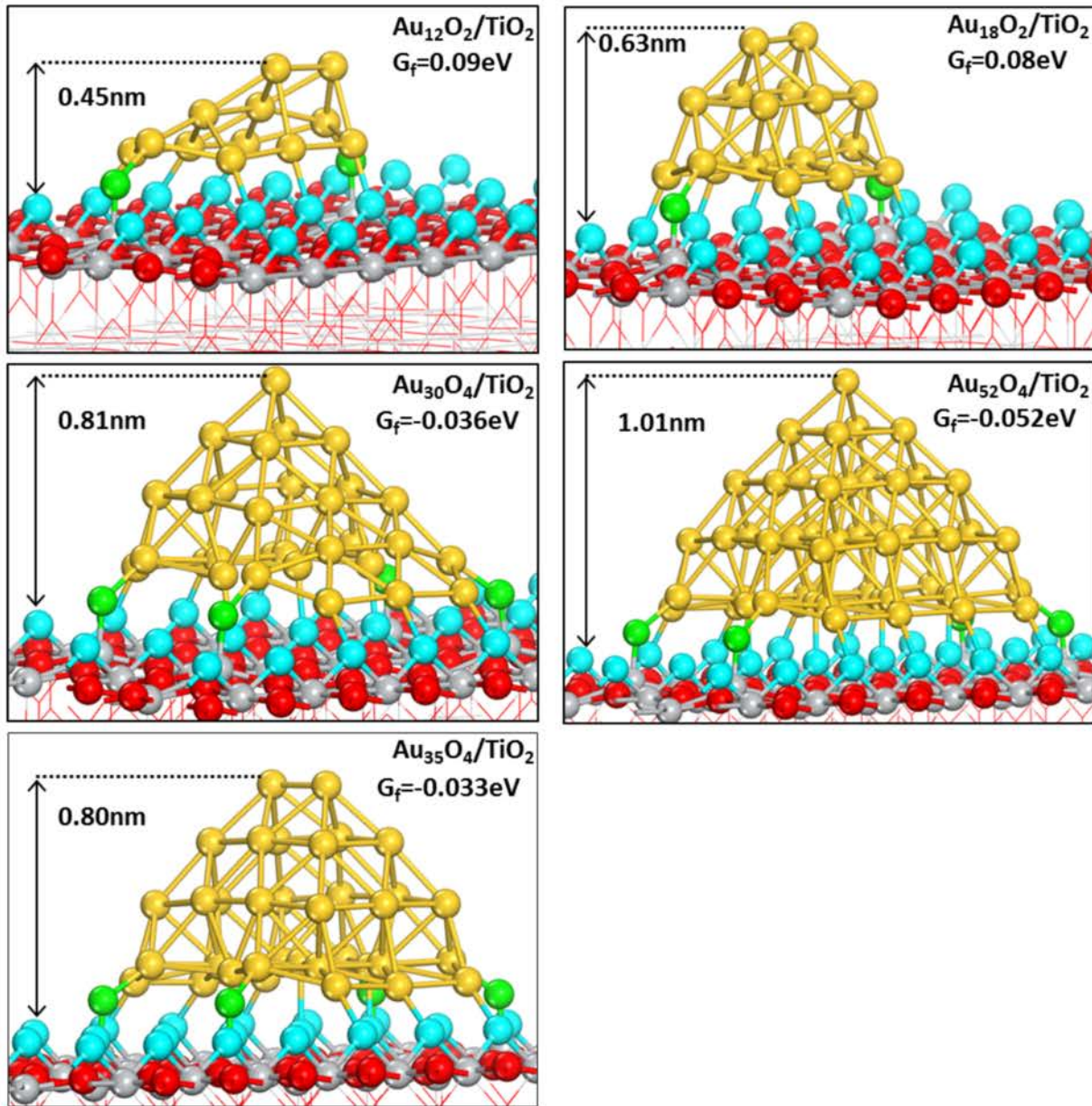
Corresponding Author: * cshang@fudan.edu.cn; *zpliu@fudan.edu.cn

PART 1 | The global minima of $\text{Au}_n\text{O}_m/\text{TiO}_2$



Supplementary Figure S1 | The slab model for calculated and most stable Au_n structures on stoichiometric and defective TiO_2 surfaces from SSW-NN global search, including the GM structures of $\text{Au}_n\text{O}_{-1}/\text{TiO}_2$ ($n=12, 18, 24$); the GM structures of Au_n/TiO_2 ($n=12, 18, 24$). The upper two figure show the slab model of p(9x3) rutile (110) surface that used in the global potential energy surface exploration of $\text{Au}_n\text{O}_m/\text{TiO}_2$ catalysts.

As shown in Figure S1, the GMs of $\text{Au}_n\text{O}_{-1}/\text{TiO}_2$ and Au_n/TiO_2 ($n=12, 18$ and 24) all exhibit stick configurations growing in the groove between two protruding rows of bridge O (O_{br}) on $\text{TiO}_2(110)$ along $[1\bar{1}0]$, anchored by eight Au- O_{br} bonds. For all $\text{Au}_n\text{O}_{-1}/\text{TiO}_2$ catalysts, the configuration of Au is largely the same as the corresponding Au_n/TiO_2 , but it is noted that the Au particles are at the distal site away from the surface O_{br} vacancy, which is different from very small clusters (e.g. Au_1 to Au_3) that sits at the O_{br} vacancy.¹⁻³



Supplementary Figure S2 | The most stable Au_nO_m structures on TiO_2 surfaces from SSW-NN global search, including the GM structures of $\text{Au}_n\text{O}_2/\text{o-TiO}_2$ ($n=12, 18$) and the GM structure of $\text{Au}_n\text{O}_4/\text{TiO}_2$ ($n=30, 35, 52$)

For O-containing Au particles (Figure S2), the GMs of $\text{Au}_{12}\text{O}_2/\text{TiO}_2$ and $\text{Au}_{18}\text{O}_2/\text{TiO}_2$ contain two $\text{Au}_{\text{ad}}\text{-Ti}_{5c}$ species at the interface. Comparing with $\text{Au}_{12}/\text{TiO}_2$ and $\text{Au}_{18}/\text{TiO}_2$, the O-containing particles, although still in the groove between two rows of O_{br} , become less spreading along $[1\bar{1}0]$ (forming only six $\text{Au}-\text{O}_{\text{br}}$ bonds) and thus higher with respect to surface. The particles have hollow voids but sealed at the bottom (Au_{18}O_2). The GM of Au_{30}O_4 cluster ($G_f = -0.035$) can be regarded as an in-between structure from Au_{24}O_4 ($G_f = -0.037$) to Au_{35}O_4 ($G_f = -0.033$). For the GM of Au_{52}O_4 , the Au particle is 1.3 nm in diameter and 1.01 nm in height with 5 atomic layers. The top 4 layers are close packed regular-square-pyramid, exposing (100) surface at the bottom. The pyramid then links with the bottom (5th) layer, a close-packed (111) plane, that is in contact with TiO_2 .

■ The coverage of Au particles on the TiO_2 (110) surface.

The coverage is defined by the total number of Au atoms in particle (3D structure) as previously used in the literature¹⁰. Hence, the coverage of 71% is in fact not high and here it corresponds to the case of supported Au_{52} , which still have a separation of 9.38 Å between adjacent clusters. The Au_{24}O_4 clusters corresponds to a coverage of 33% in this definition, which have a separation of 9.5 Å between clusters.

■ The formation energy of Au_nO_m (G_f) computation.

The formation energies of gold are calculated using equation (S1), where $G[X]$ is the approximate Gibbs free energy of X. For solids, the free energy is approximated by its DFT total energy. For molecules, the free energy is calculated as equation (S2), including the DFT total energy [X], the zero-point-energy (ZPE) and the thermodynamic correction terms. $G[\text{Au}_{(111)}]$ is the free energy of a surface Au atom on $\text{Au}(111)$.

$$\Delta G_{\text{Au}} = \{G[\text{Au}_n\text{O}_m/\text{TiO}_2] - G[\text{TiO}_2]\} - n \times G[\text{Au}_{(111)}] - m/2 \times G[\text{O}_2]/n \quad (\text{S1})$$

$$G[X](p, T) = E[X] + ZPE[X] + [\mathbf{H}[X](p^0, T) - \mathbf{H}[X](p^0, 0\text{K})] - TS[X](p^0, T) + k_B T \ln \frac{p}{p^0} \quad (\text{S2})$$

■ The determination of the optimal O contents on/in Au particles

To determine the optimal oxygen content on/in Au particles, we have computed the differential adsorption energy of O_{ad} atom (ΔG) on the $\text{Au}_n\text{O}_m/\text{TiO}_2$ catalysts using equation (S3) under ambient condition. $G[\text{Au}_n\text{O}_x/\text{TiO}_2]$ and $G[\text{Au}_{n-1}\text{O}_{x-1}/\text{TiO}_2]$ are the total energy of the identified GM structures. The result is shown in Table S1, where the positive value means that the oxygen is more stable in the gas phase than on the surface.

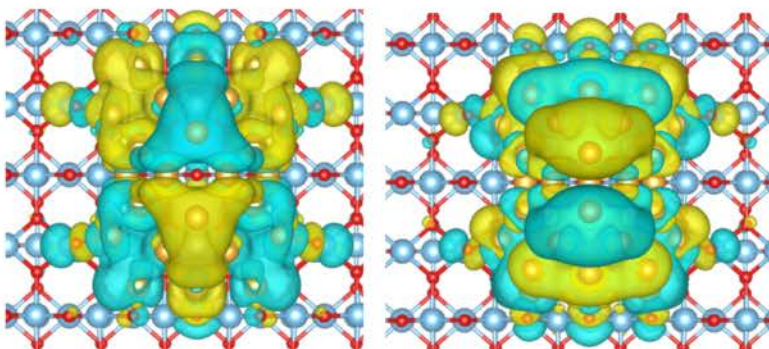
$$\Delta G_{x0} = G[\text{Au}_n\text{O}_x/\text{TiO}_2] - G[\text{Au}_{n-1}\text{O}_{x-1}/\text{TiO}_2] - 1/2 * G[\text{O}_2] \quad (\text{S3})$$

Supplementary Table S1 | The differential adsorption energies of O in $\text{Au}_n\text{O}_x/\text{TiO}_2$.

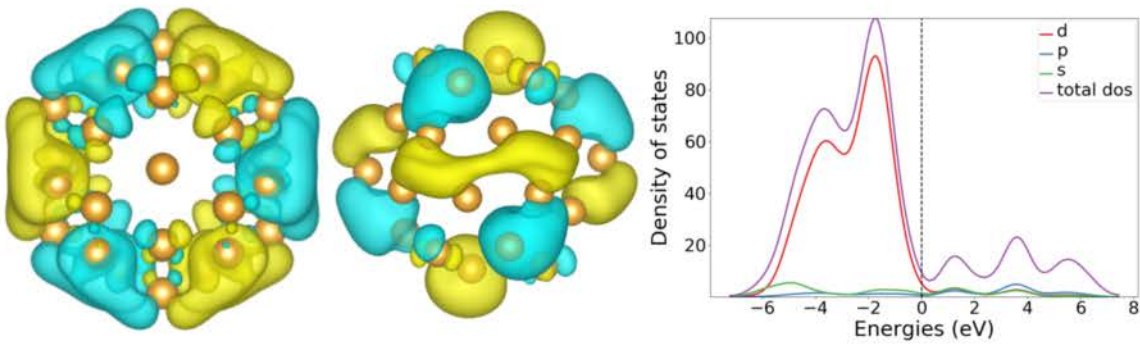
	Au ₆	Au ₁₂	Au ₁₈	Au ₂₄
ΔG_{10}	-0.30	-1.27	-1.15	-1.02
ΔG_{20}	0.26	-0.62	-1.09	-1.39
ΔG_{30}	/	1.17	0.12	-0.72
ΔG_{40}	/	/	/	-0.32
ΔG_{50}	/	/	/	0.80

■ The LUMO wavefunction of Au_{24}O_4 and Au_{37}O_4 ,

In Supplementary Figure S3 and S4, we show the LUMO wavefunction of the nano-domes, $\text{Au}_{24}\text{O}_4/\text{TiO}_2$ and Au_{37}O_4 , and compare them with the HOMO and LUMO of Au_{32} hollow cage in the gas phase. We found that the LUMO of the dome structures has the delocalized characteristics, demonstrating the aromaticity similar to Au_{32} cage. The density of states plotted in Supplementary Figure S4 indicates that the HOMO of Au_{32} cage is composed mainly by 5d orbitals but the LOMO is contributed from both 5d and 6s orbitals.



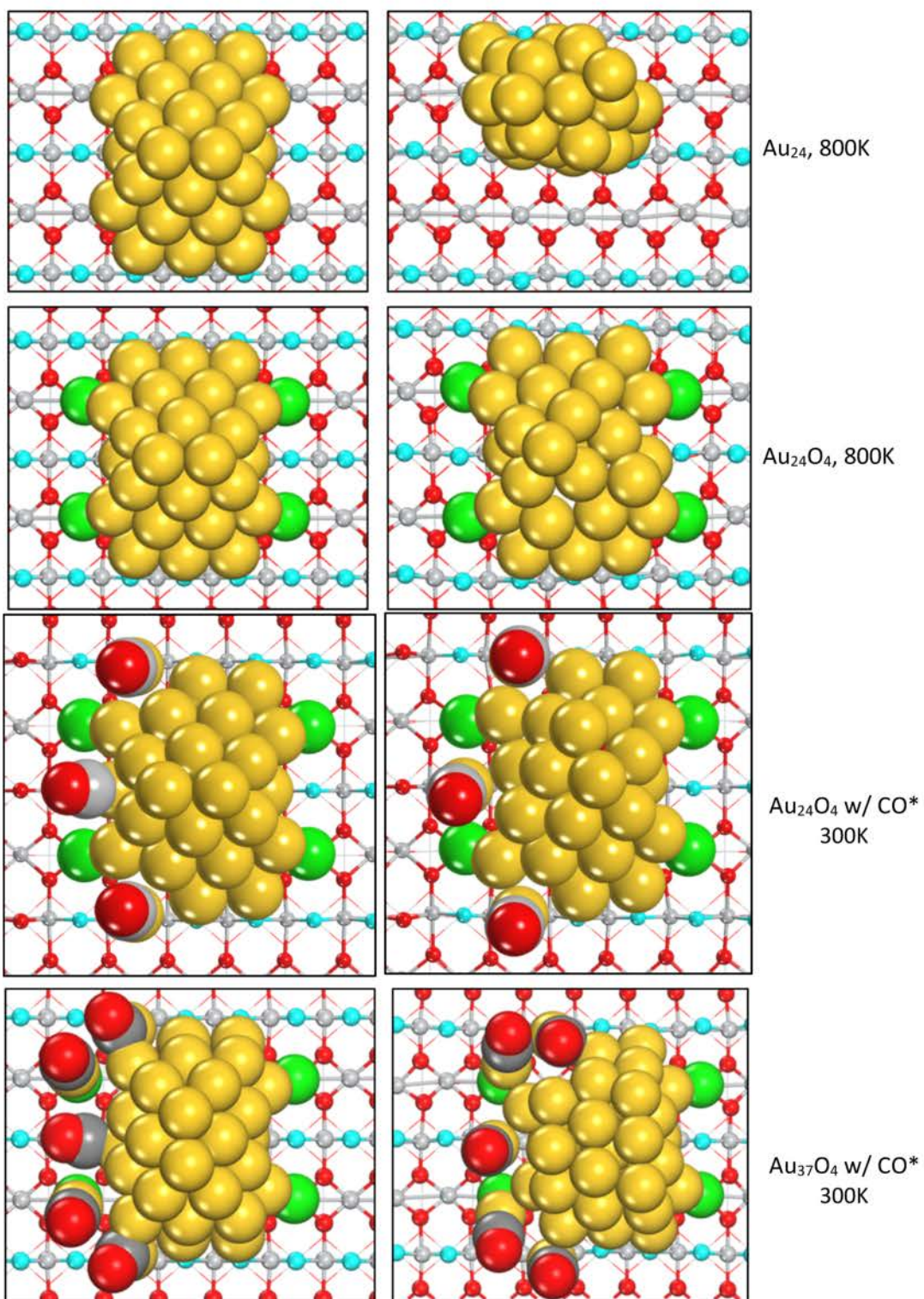
Supplementary Figure S3 | Lowest unoccupied orbital (LUMO) for $\text{Au}_{24}\text{O}_4/\text{TiO}_2$ and Au_{37}O_4 . This state is critical since it helps to stabilize O_{br} vacancy.



Supplementary Figure S4 | HOMO (left), LUMO (middle) and p-DOS of Au₃₂ hollow cage (right).

The HOMO of Au₃₂ is mainly contributed by Au 5d orbitals and LUMO have contributions from both 6s and 5d orbitals.

In Supplementary Figure S5, we show the initial and final snapshots of Au₂₄O₄/TiO₂, Au₂₄/TiO₄ from MD simulation at 800 K for 1 ns. The morphology of Au₂₄O₄/TiO₂ catalyst basically keeps the configuration of the GM. For Au₂₄/TiO₄, the cluster has completely lost its original dome-like morphology, migrating away from the original site. We have also shown the initial and final snapshots of Au₂₄O₄/TiO₂ and Au₃₇O₄/TiO₂ from MD simulation at 300 K for 1 ns, where the clusters basically maintain its original morphology which atoms slightly vibration around its initial position.



Supplementary Figure S5 | The initial (left panel) and final snapshots (right panel) for Au_{24} , Au_{24}O_4 and Au_{37}O_4 particles with (w/) or without the adsorption of CO from MD simulations at 800K or 300K for 1ns. A movie corresponds to the MD trajectory of Au_{24}O_4 / TiO_2 is also present where each frame corresponds to 10 ps.

PART 2 | Energetics data and microkinetic simulation details for CO oxidation on $\text{Au}_n\text{O}_m/\text{TiO}_2$

Supplementary Table S2 lists the formation energy of O_{br} vacancy, the adsorption energy of CO and the reaction barrier for CO to react the O_{br} of different $\text{Au}_n\text{O}_m/\text{TiO}_2$ catalysts. Table S3 lists the reaction energy barrier and reaction rate constant used for microkinetic simulation of CO oxidation on Au/TiO_2 at $p(\text{CO}) = 0.01\text{atm}$, $p(\text{O}_2) = 0.21\text{atm}$ and 300K .

Supplementary Table S2 | Formation energy of O_{br} vacancy next to Au particle ($E_{\text{f}}-\text{O}_{\text{br}}$), the adsorption energy of CO ($E_{\text{ad}-\text{CO}}$) and the barrier of CO to react with O_{br} (E_b). All are in the unite of eV.

	Au_6O	Au_{12}O_2	Au_{18}O_2	Au_{24}O_4	Au_{37}O_4	Au_{52}O_4
$E_{\text{f}}-\text{O}_{\text{br}}^*$	2.31	2.70	2.63	1.66	2.08	2.21
$E_{\text{ad}-\text{CO}}^a$	1.15	1.33	0.53	1.01	0.22	0.23
E_b^b	0.93	0.93	0.45	0.61	0.16	0.17

a: E_{ad} of CO in the initial state of the first reaction step, $\text{CO}^*+\text{O}_{\text{br}}$.

b: The reaction barrier for CO to react with O_{br} (the first step, $\text{CO}^*+\text{O}_{\text{br}}$).

*: PBE+U functional is utilized for computing the O vacancy formation energy.

Supplementary Table S3 | The free energy barrier ($G_{a,+}$ and $G_{a,-}$) and reaction rate constant (k_+ , k_-) used for microkinetic simulation of CO oxidation on Au/TiO_2 at $p(\text{CO}) = 0.01\text{atm}$, $p(\text{O}_2) = 0.21\text{atm}$ and 300K . The initial coverage for Au sites (*) and reactive O_{br} (O\$) are set to 1. The initial coverage for O_v (\$), Au site (^) with O_2 adsorbed in O_v (O_2)$ are set to zero.

Elementary step Au_{24}O_4	$G_{a,+}$	$G_{a,-}$	k_+	k_-
$\text{CO} + * \rightarrow \text{CO}^*$	0.52	1.10	1.15E+01	2.07E-06
$\text{CO}^* + \text{O\$} \rightarrow \text{CO}_2 + * + \$$	0.57	2.17	1.66E+03	2.19E-24
$\text{O}_2 + \$ + * \rightarrow \text{O}_2\$ + ^$	0.54	1.01	5.29E+03	6.73E-05
$\text{CO} + ^ \rightarrow \text{CO}^{\wedge}$	0.52	0.81	1.15E+04	4.83E-02
$\text{CO}^{\wedge} + \text{O}_2\$ \rightarrow \text{OCOO}^{\wedge}\$$	0.32	0.48	3.87E+07	5.39E+04
$\text{OCOO}^{\wedge}\$ \rightarrow \text{CO}_2 + \text{O\$} + *$	0.29	4.43	1.21E+07	2.35E-62

Elementary step Au_{37}O_4	$G_{a,+}$	$G_{a,-}$	k_+	k_-
$\text{CO} + * \rightarrow \text{CO}^*$	0.52	0.26	1.15E+01	2.68E+08
$\text{CO}^* + \text{O\$} \rightarrow \text{CO}_2 + * + \$$	0.13	1.27	4.09E+10	2.88E-09
$\text{O}_2 + \$ + * \rightarrow \text{O}_2\$ + ^$	0.54	1.77	5.29E+03	1.15E-17
$\text{CO} + ^ \rightarrow \text{CO}^{\wedge}$	0.52	0.18	1.15E+04	5.91E+09
$\text{CO}^{\wedge} + \text{O}_2\$ \rightarrow \text{OCOO}^{\wedge}\$$	0.28	0.68	1.24E+08	2.35E+01
$\text{OCOO}^{\wedge}\$ \rightarrow \text{CO}_2 + \text{O\$} + *$	0.34	4.58	1.21E+07	7.10E-65

The reaction condition is set as $p(\text{CO}) = 0.01\text{atm}$, $p(\text{O}_2) = 0.21\text{ atm}$, and a series of temperature utilized in simulations, ranging from 200 to 300 K. The catalysts initially have all the interfacial Au sites occupied by adsorbed CO; the surface is in stoichiometry without O_v and O_2 coverage on surface is zero.

Computation for reaction rate ($\text{mol}_{\text{CO}} \text{g}_{\text{Au}}^{-1} \text{s}^{-1}$). The reaction rate of CO_2 production on Au_{24}O_4 and Au_{37}O_4 is obtained from equation S4, where R_{mk} is the rate obtained from microkinetic simulation. Each Au_n ($n=24, 37$) particle has two active sites at the interface and the Au molar mass is 197 g/mol.

$$R(\text{Au}_n, n=24, 37) = R_{\text{mk}} * 2/n/197 = 4.50 * 10^{-2} \text{ mol}_{\text{CO}} \text{ g}_{\text{Au}}^{-1} \text{ s}^{-1} \quad (\text{S4})$$

RMSD computation. The RMSD of Au particle during MD simulation is calculated by equation (S5), where q_i is the cartesian coordinates of atom i.

$$\text{RMSD} = \sqrt{\left(\sum q_i^t - q_i^0 \right)^2 / n_{\text{Au}}} \quad (\text{S5})$$

Supplementary Table S4 | The benchmark of the dispersion effect (with Grimme's D3 dispersion correction, PBE-D3)⁴, the dipole effect and the layer effect .

	Au ₂₄ O ₄			Au ₃₇ O ₄		
	PBE+U	PBE+U, D3	PBE+U, D3, Dipole ^g	PBE+U, D3, 5L ^{d, g}	PBE+U	PBE+U, D3
E _{ad} -CO ^a	1.10	1.11	1.12	1.14	0.26	0.29
E _{b1} ^b	0.57	0.55	0.57	0.57	0.13	0.15
E _{ad} -CO ^c	0.81	0.76	0.79	0.78	0.18	0.16
E _{ad} -O ₂ ^c	1.01	1.04	1.02	1.05	1.77	1.76
E _{b2} ^b	0.32	0.27	0.28	0.25	0.28	0.32
E _{b3} ^c	0.29	0.32	0.30	0.26	0.34	0.32

a: E_{ad} of CO in the initial state of the first reaction step, CO*+O_{br}.

b,e,f: The reaction barrier for three steps.

c: E_{ad} of CO and O₂ in the state of the second reaction step

d: 5L indicates the TiO₂ with 5 layers

g: a single point energy is computed using the configuration from PBE+U+D3.

As shown in Table S4, the variation of the adsorption energy and energy barrier of key reactions are within 0.05 eV with or without dispersion correction and dipole correction, which doesn't affect the main conclusion.

PART 3 | Training dataset and benchmark of the AuTiO and AuTiCO G-NN potential

To cover all the likely compositions of Au-Ti-O our SSW simulations have been carried out for different structures (including bulk, layer and particle), compositions and atom number per unit cell (4 ~ 524) for Ti, TiO, Au, AuO_x and Au-Ti-O. Overall, these exhaustive SSW simulations generate more than 10⁷ structures on global PES. The final global dataset that is computed from high accuracy DFT calculation contains 44,541 structures screened from global PES, as detailed in SI Table S4.

To pursue a high accuracy for PES, we have adopted a large set of power-type structure descriptors (PTSDs), which contains 198 descriptors for every element with only power-type structure descriptors, including 82 two-body, 96 three-body, 20 four-body descriptors, and compatibly, the network utilized is also large involving two-hidden layers (198-50-50-1 network), equivalent to 37,753 network parameters in total. Min-max scaling is utilized to normalization the training data sets. Hyperbolic tangent activation functions were used for the hidden layers, while a linear transformation was applied to the output layer of all networks. The limited-memory Broyden-Fletcher-Goldfarb-Shannon (L-BFGS) method is used to minimize the loss function to match DFT energy, force and stress. The final energy and force criterions of the root mean square errors are around 6.3 meV/atom and 0.155 eV/Å respectively. To confirm the accuracy of G-NN PES for Au particles on TiO₂, we also select key Au/TiO₂ structures to compare G-NN results with DFT calculations. It has a max energy error of 3.89 meV/atom, which is quite standard for NN potentials and accurate enough (correct energy ordering) for searching the stable structure candidates. This benchmark results can be found in SI Table S6.

Finally, SSW-NN simulation is performed over a wide range of composition and structures, both for the global dataset generation in Fig. 1 and for the PES. For the data in Fig. 1, they are taken from the global minima of AuTiO as identified from the SSW-NN simulation, where each composition is simulated in the unit cells of 330 ~ 525 atoms and explored to visit more than 10⁵ minima on PES

by SSW. Thus, a large variety of structures have been obtained from SSW-NN simulation. All the low energy structure candidates from SSW-NN exploration are finally fully optimized and verified by DFT calculations.

Supplementary Table S4 lists the structure information in the first principles global dataset for AuTiO G-NN potential training. Taking this dataset as basic training set, we then add extra data involving carbon element, including CO and O₂ adsorbed on identified Au₂₄O₄ and Au₃₇O₄ clusters. Supplementary Table S5 lists the structure information in the first principles global dataset for AuTiCO G-NN potential training. Benchmark between G-NN and DFT calculations for several supported Au_nO_m/TiO₂ catalysts are listed in Table S6.

■ Training dataset of the AuTiO G-NN potential

All the structures included in the dataset are sorted in the sequence of number of C, O, Ti, Au atoms, where the structures obtained from the Bayesian optimization are listed at the bottom. All the training data sets are available online.

Supplementary Table S5 | Structure information in the first principles global dataset. Listed data are the number of the structures in the global dataset, as distinguished by the chemical formula, the number of atoms (N), the type of structures (cluster, bulk, layer).

Species	Natm	cluster	layer	bulk	total
Au8	8	0	125	0	125
Au14	14	0	3	56	59
Au15	15	135	5	69	209
Au16	16	1365	218	8165	9746
Au28	28	0	2	68	70
Au29	29	0	37	30	67
Au30	30	59	26	121	206
Au31	31	0	0	75	75
Au32	32	30	2	225	257
Au45	45	25	0	0	25
O1-Au16	17	0	1	133	134
O2-Au16	18	47	33	86	166
O4	4	0	15	0	15
O4-Au16	20	0	86	174	260
O4-Au24	28	76	18	109	203
O6-Au4	10	0	0	2918	2918
O6-Au16	22	0	5	187	192
O6-Ti4	10	0	0	44	44
O7-Au8	15	0	0	1158	1158
O7-Ti4-Au2	13	0	103	0	103
O7-Ti4-Au5	16	0	261	13	274
O8-Au8	16	0	0	2361	2361
O8-Au16	24	0	66	40	106
O8-Ti4	12	2115	190	11379	13684
O8-Ti4-Au2	14	0	115	0	115
O8-Ti4-Au5	17	0	306	12	318
O9-Ti4-Au1	14	0	153	0	153
O9-Ti4-Au5	18	0	46	240	286
O10-Au16	26	0	63	19	82
O10-Ti5-Au9	24	0	3	867	870
O11	11	0	78	24	102

O11-Ti5-Au8	24	0	0	893	893
O11-Ti6-Au2	19	0	52	99	151
O11-Ti6-Au5	22	0	52	40	92
O12-Au16	28	0	8	118	126
O12-Ti4-Au8	24	0	0	1237	1237
O12-Ti6-Au1	19	0	38	117	155
O12-Ti6-Zn5	23	0	78	196	274
O12-Ti8	20	0	0	378	378
O13-Ti6	19	0	144	476	620
O13-Ti6-Au1	20	0	11	177	188
O13-Ti6-Au5	24	0	26	1585	1611
O13-Ti7	20	0	40	19	59
O14-Au16	30	0	0	122	122
O14-Ti7	21	0	0	1	1
O14-Ti8	22	0	0	198	198
O15-Au16	31	0	0	142	142
O15-Ti9	24	0	2	283	285
O16-Ti8	24	0	127	538	665
O17-Au16	33	0	8	103	111
O18-Ti7	25	0	0	1	1
O18-Ti8	26	0	0	3	3
O18-Au12	30	0	349	17	366
O22-Au16	38	0	0	199	199
O24-Au16	40	0	0	14	14
O31-Ti16-Au4	51	0	93	0	93
O31-Ti16-Au8	55	0	64	0	64
O32-Ti16-Au4	52	0	98	0	98
O32-Ti16-Au8	56	0	58	0	58
O32-Ti16-Au16	64	0	151	0	151
O33-Ti16-Au5	54	0	182	0	182
O33-Ti16-Au7	56	0	57	0	57
O33-Ti16-Au16	65	0	125	0	125
O47-Ti24-Au2	73	0	70	0	70
O47-Ti24-Au3	74	0	48	6	54
O47-Ti24-Au8	79	0	49	0	49
O47-Ti24-Au20	91	0	48	0	48
O48-Ti24-Au1	73	0	69	0	69
O48-Ti24-Au3	75	0	69	0	69
O48-Ti24-Au8	80	0	52	0	52
O48-Ti24-Au12	84	0	43	0	43
O52-Ti24-Au1	77	0	68	0	68
O52-Ti24-Au2	78	0	65	0	65
O52-Ti24-Au12	88	0	43	0	43
O52-Ti24-Au20	96	0	101	0	101
O63-Ti32-Au8	103	0	77	0	77
O63-Ti32-Au14	109	0	22	0	22
O64-Ti32-Au8	104	0	50	0	50
O64-Ti32-Au14	110	0	13	0	13
O64-Ti32-Au8	105	0	77	0	77
O65-Ti32-Au14	111	0	24	0	24

O218-Ti108-Au18	344	0	7	0	7
O218-Ti108-Au24	350	0	10	0	10
O324-Ti162-Au24	510	0	56	0	56
O324-Ti162-Au30	516	0	2	0	2
O324-Ti162-Au36	522	0	4	0	4
O326-Ti162-Au24	512	0	9	0	9
O326-Ti162-Au30	518	0	5	0	5
O326-Ti162-Au36	524	0	4	0	4
O327-Ti162-Au24	513	0	77	0	77
O328-Ti162-Au24	514	0	29	0	29
O329-Ti162-Au24	515	0	6	0	6
total	--	3580	4969	35722	44541

■ Training dataset of the AuTiCO G-NN potential

Supplementary Table S6 | Structure information in the first principles global dataset utilized in G-NN training. Listed data are the number of the structures in the global dataset, as distinguished by the chemical formula, the number of atoms (N), the type of structures (cluster, bulk, layer).

Species	Natm	cluster	layer	bulk	total
Au8	8	0	125	0	125
Au14	14	0	3	56	59
Au15	15	135	5	69	209
Au16	16	1362	217	8165	9744
Au28	28	0	2	68	70
Au29	29	0	37	30	67
Au30	30	59	26	121	206
Au31	31	0	0	75	75
Au32	32	30	2	225	257
Au45	45	25	0	0	25
O1	1	1	0	0	1
O1-Au16	17	0	1	133	134
O2	2	5	0	0	5
O2-Au16	18	0	49	187	236
O3-Au16	19	47	33	86	166
O4	4	0	15	0	15
O4-Au16	20	0	85	174	259
O4-Au24	28	76	18	109	203
O6-Au4	10	0	0	2918	2918
O6-Au16	22	0	5	169	174
O6-Ti4	10	0	0	44	44
O7-Au8	15	0	0	1158	1158
O7-Ti4-Au2	13	0	103	0	103
O7-Ti4-Au5	16	0	261	13	274
O8-Au8	16	0	0	2361	2361
O8-Au16	24	0	65	39	104
O8-Ti4	12	2115	190	11379	13684
O8-Ti4-Au2	14	0	115	0	115
O8-Ti4-Au5	17	0	306	12	318
O9-Ti4-Au1	14	0	153	0	153
O9-Ti4-Au5	18	0	46	240	286
O10-Au16	26	0	61	19	80

O10-Ti5-Au9	24	0	3	867	870
O11	11	0	77	24	101
O11-Ti5-Au8	24	0	0	893	893
O11-Ti6-Au2	19	0	52	99	151
O11-Ti6-Au5	22	0	52	40	92
O12-Au16	28	0	7	105	112
O12-Ti4-Au8	24	0	0	1237	1237
O12-Ti6-Au1	19	0	38	117	155
O12-Ti6-Zn5	23	0	78	196	274
O12-Ti8	20	0	0	378	378
O13-Ti6	19	0	144	476	620
O13-Ti6-Au1	20	0	11	177	188
O13-Ti6-Au5	24	0	26	1585	1611
O13-Ti7	20	0	40	19	59
O14-Au16	30	0	0	119	119
O14-Ti7	21	0	0	1	1
O14-Ti8	22	0	0	198	198
O15-Au16	31	0	0	133	133
O15-Ti9	24	0	2	283	285
O16-Ti8	24	0	127	538	665
O17-Au16	33	0	8	99	107
O18-Ti7	25	0	0	1	1
O18-Ti8	26	0	0	3	3
O18-Au12	30	0	349	17	366
O22-Au16	38	0	0	199	199
O24-Au16	40	0	0	14	14
O31-Ti16-Au4	51	0	93	0	93
O31-Ti16-Au8	55	0	64	0	64
O32-Ti16-Au4	52	0	98	0	98
O32-Ti16-Au8	56	0	58	0	58
O32-Ti16-Au16	64	0	150	0	150
O33-Ti16-Au5	54	0	181	0	181
O33-Ti16-Au7	56	0	57	0	57
O33-Ti16-Au16	65	0	125	0	125
O47-Ti24-Au2	73	0	70	0	70
O47-Ti24-Au3	74	0	48	6	54
O47-Ti24-Au8	79	0	49	0	49
O47-Ti24-Au20	91	0	48	0	48
O48-Ti24-Au1	73	0	69	0	69
O48-Ti24-Au3	75	0	69	0	69
O48-Ti24-Au8	80	0	52	0	52
O48-Ti24-Au12	84	0	43	0	43
O52-Ti24-Au1	77	0	68	0	68
O52-Ti24-Au2	78	0	65	0	65
O52-Ti24-Au12	88	0	43	0	43
O52-Ti24-Au20	96	0	101	0	101
O63-Ti32-Au8	103	0	77	0	77
O63-Ti32-Au14	109	0	22	0	22
O64-Ti32-Au8	104	0	50	0	50
O64-Ti32-Au14	110	0	13	0	13

O65-Ti32-Au8	105	0	77	0	77
O65-Ti32-Au14	111	0	24	0	24
O218-Ti108-Au18	344	0	7	0	7
O218-Ti108-Au24	350	0	10	0	10
C1-Ti25	26	0	5	0	5
C1-Ti26	27	0	45	232	277
C1-O15-Ti7	23	0	112	277	389
C1-O15-Ti8	24	0	480	436	916
C1-O16-Ti8	25	0	618	421	1039
C1-O25-Ti12-Au5	43	0	193	0	193
C1-O25-Ti12-Au6	44	0	87	0	87
C1-O26-Ti12-Au4	43	0	177	0	177
C1-O26-Ti12-Au5	44	0	443	0	443
C1-O26-Ti12-Au6	45	0	298	0	298
C2-Ti25	27	0	100	486	586
C2-O15-Ti8	25	0	122	292	414
C2-O16-Ti8	26	0	575	488	1063
C2-O50-Ti24-Au10	86	0	26	0	26
C2-O50-Ti24-Au12	88	0	16	0	16
C2-O52-Ti24-Au8	86	0	13	0	13
C2-O52-Ti24-Au10	88	0	77	0	77
C2-O52-Ti24-Au12	90	0	37	0	37
C3-O16-Ti8	27	0	576	453	1029
C4-Ti23	27	0	1	0	1
C8	8	0	16	241	257
C10-O6-Ti3	19	0	117	465	582
C13-O8-Ti4	25	0	314	309	623
C20-O12-Ti6	38	0	4	428	432
C26-O16-Ti8	50	0	3	319	322
C1-O217-Ti108-Au24	350	0	11	0	11
C1-O219-Ti108-Au24	352	0	10	0	10
C1-O220-Ti108-Au24	353	0	34	0	34
C1-O221-Ti108-Au24	354	0	72	0	72
C1-O222-Ti108-Au24	355	0	161	0	161
C2-O223-Ti108-Au24	357	0	40	0	40
C6-O225-Ti108-Au24	363	0	100	0	100
C6-O226-Ti108-Au35	375	0	100	0	100
total	--	3855	9751	40531	54127

■ Benchmark between G-NN and DFT calculations for supported $\text{Au}_n\text{O}_m/\text{TiO}_2$ catalysts.

Supplementary Table S7 |. Benchmark between G-NN and DFT calculations for supported Au/TiO_2 systems. The lowest energy in each sequence is the GM, defined as zero. Listed data include the compositions, total atom number (N_{atom}), DFT energy, NN energy and energy differences between DFT energy and NN energy (E_{diff} , meV/atom)

composition	Natom	DFT-en (eV)	NN-en (eV))	en-diff (meV/atom)
	0	-1.185	2.332	

$\text{Au}_{18}\text{O}_2/\text{TiO}_2$	506	0.917	-0.803	3.398
		1.293	-0.625	3.791
		0	-1.772	3.462
$\text{Au}_{24}\text{O}_4/\text{TiO}_2$	514	0.476	-1.415	3.698
		0.733	-1.298	3.891
		0	-1.848	3.566
$\text{Au}_{30}\text{O}_2/\text{TiO}_2$	518	0.007	-1.811	3.509
		0.041	-1.750	3.456
		0	-1.464	4.135
$\text{Au}_{24}\text{O}_4/\text{TiO}_2\text{-CO}$	354	0.230	-1.170	3.966
		0.699	-0.944	4.633
$\text{Au}_{37}\text{O}_4/\text{TiO}_2\text{-5CO}$	537	0	-2.663	4.959
$\text{Au}_{24}\text{O}_4/\text{TiO}_2\text{-4CO}$	522	0	-0.700	1.341
$\text{Au}_{37}\text{O}_4/\text{TiO}_2\text{-4CO}$	535	0	2.887	5.396

■ Supplementary References

1. Matthey, D. *et al.* Enhanced Bonding of Gold Nanoparticles on Oxidized $\text{TiO}_2(110)$. *Science* **315**, 1692 (2007).
2. Wahlstrom, E. *et al.* Bonding of gold nanoclusters to oxygen vacancies on rutile $\text{TiO}_2(110)$. *Phys. Rev. Lett.* **90** (2003).
3. Chen, M. S. & Goodman, D. W. Catalytically active gold: From nanoparticles to ultrathin films. *Acc. Chem. Res.* **39**, 739-746 (2006).
4. Grimme, S., Antony, J., Ehrlich, S. & Krieg, H. A consistent and accurate ab initio parametrization of density functional dispersion correction (DFT-D) for the 94 elements H-Pu. *J. Chem. Phys.* **132** (2010).